# Wide-field Kerr Microscopy and Magnetometry on $Cr_2Ge_2Te_6$ exfoliated van-der-Waals flakes

**IVAN SOLDATOV[1], BURAK ÖZER[1,2], SAICHARAN ASWARTHAM[1], SEBASTIAN SELTER[1], LOUIS VEYRAT[1,2,3], BERND BÜCHNER[1], and RUDOLF SCHÄFER[1] (Senior Member, IEEE)**

[1]Leibniz Institute for Solid State and Materials Research Dresden, Helmholtzstrasse 20, D-01069 Dresden, Germany
[2]Würzburg-Dresden Cluster of Excellence ct.qmat, Dresden, Germany
[3]Now at: Nano & semiconductor group, LNCMI-Toulouse, 143 Avenue de Rangueil, 31400 Toulouse, France

Corresponding author: R. Schäfer (e-mail: r.schaefer@ifw-dresden.de)

This work was supported by the German Research Foundation (DFG) under Germanys Excellence Strategy through the Dresden-Würzburg Cluster of Excellence on Complexity and Topology in Quantum Matter — ct.qmat (EXC 2147, project-id 390858490). L.V. was supported by the Leibniz Association through the Leibniz Competition. S.A. was supported by DFG, funding number DFG AS 523/4-1

**ABSTRACT** The potential of wide-field magneto-optical Kerr microscopy for the characterisation of low-dimensional van-der-Waals crystals is explored using the example of $Cr_2Ge_2Te_6$ flakes in the ten nanometers thickness range. Although the magnetic domains with an expected width in the hundred-nanometer range cannot be seen on this material due to the limited lateral resolution, we show that Kerr microscopy is nevertheless a very valuable method for measuring the magnetization loops on selectable thickness regions on the flake. From the loop character one can indirectly infer on the existence or suppression of band domains, which are the equilibrium patterns above a film thickness of about 7 nm. We derived this characteristic thickness from the initial susceptibility of the hysteresis loops and used it to estimate the specific domain wall energy to be $2.7 \cdot 10^{-4}$ J/m$^2$. We further demonstrate a thickness- and light colour dependent sign inversion of the Kerr signal that is explained by a Fresnel-type depth sensitivity concept. Accordingly, the Kerr contrast is governed by the relative phase of the Kerr amplitude that can be freely adjusted by a rotatable compensator. The compensator is thus the decisive optical element in magneto-optical Kerr magnetometry and microscopy on low-dimensional materials. It needs to be appropriately aligned to avoid a cancelation of the Kerr contrast and to maximise the Kerr signal.

**INDEX TERMS** Magnetic domains, magnetic hysteresis, magneto-optical Kerr microscopy, MOKE magnetometry, 2D magnetic materials, van der Waals materials

## I. INTRODUCTION

Since their discovery about ten years ago [1], [2], ferromagnetically ordered two-dimensional (2D) van-der-Waals (vdW) materials, exfoliated like graphene via an adhesive tape from bulk crystals [3], have been intensively explored. Examples are $CrBr_3$, $CrI_3$, $Cr_2Ge_2Te_6$, or $Fe_3GeTe_2$ flakes with thicknesses ranging between monolayers to a few layers. Such 2D vdW materials often have ferromagnetic transition temperatures well below room temperature and they are characterized by a uniaxial magnetic anisotropy perpendicular to the film plane. Details on the numerous material classes, their properties, and characterization tools can be found in several comprehensive review articles [4]–[7].

As for most magnetic materials, magnetic hysteresis measurements and domain research also play crucial roles in the characterization and understanding of 2D van der Waals materials and have therefore been used from the very beginning[1]. *Hysteresis loops* in perpendicular fields are mostly obtained by polar Magneto-Optical Kerr Effect (MOKE) magnetometry in laser-based MOKE setups[2] [1], [2], [10]–[19] or by applying (anomalous) Hall effect transport measurements [13], [20]–[24]. MOKE magnetometry leads to *local* loops by plotting the reflected Kerr signal of a focused, micrometer-sized laser beam as a function of an applied magnetic field. For exfoliated flake specimens, which normally

[1]Note that many published data were obtained on exfoliated vdW flakes with thicknesses of several tens of nanometers and beyond. Such specimens may not be called "2D" anymore in the sense that magnetic order in ultrathin films should actually be destroyed due to thermal fluctuations (Mermin-Wagner theorem) but can nevertheless exist if strong magnetic anisotropy is present as it may be true for van-der-Walls materials.

[2]Besides the Kerr effect, also other magneto-optical effects can be applied to study 2D materials [8], [9].

consist of areas with different thickness, it has the advantage that a specific thickness can be selected. This is not true for Hall magnetometry, which results in *integral* loops. For the latter, the electrical resistance of a flake structured in a Hall bar geometry is measured, which is only possible with electrically conductive media. For magnetic *domain imaging* on vdW flakes mostly Lorentz Transmission Electron Microscopy (LTEM) [22], [25]–[34], novel Nitrogen-Vacancy Scanning Microscopy (NVSM) [17], [35]–[37], and X-ray based imaging (X-ray Photoemission Electron Microscopy, XPEEM [15], [26], [38], and Scanning Transmission X-ray Microscopy, STXM [30], [39], [40]), have been applied. Notably is also a special scanning method in which a SQUID (Superconducting Quantum Interference Device) sensor is integrated on an atomic force microscope tip [41], [42] thus sensing the magnetic stray field emerging from the domains as for the NVSM method. Most observations were made on $Fe_3GeTe_2$ and $Cr_2Ge_2Te_6$ layers, followed by $CrI_3$ and $CrBr_3$. Various thickness- and field-dependent domain patterns were observed, which are also known from other magnetic films with perpendicular anisotropy, including band domains (narrow up-and-down magnetized domains in a straight or maze arrangement) and bubble domains (perpendicularly magnetized domains in cylindrical shape) with sizes in the 100 nm regime. Also skyrmion-like structures (bubble domains with Néel-like domain walls) were found or predicted when 2D films were combined with proper heavy metal layers in heterostructures [22], [24], [26], [30], [43]–[45], making 2D vdW films interesting candidates for spintronic devices.

The goal of our work is to explore the potential of *wide-field Kerr microscopy* for domain imaging and magnetometry on 2D magnetic vdW materials. It is a widely-used in-lab technique that is based on an optical polarization microscope with the advantage that magnetic domains at a certain sample area can be readily seen without much experimental effort [46] compared to, e.g., synchrotron- or electron microscopy based imaging methods. Also magnetization loops can be easily obtained by plotting the Kerr intensity at selectable sample areas as a function of an applied magnetic field [47]. The hysteresis loops can then be conveniently interpreted because the domains responsible for them are known. Interestingly, only a few reports on magnetic vdW materials using this technique have been published to date: Polar wide-field Kerr microscopy was applied by *Yin et al.* [18] to study $Fe_3GeTe_2$ flakes with thicknesses between 10 and 110 nm, claiming to see a change from wide domains to maze domains with increasing thickness[3]. The authors made full use of their Kerr microscope by combining imaging with local hysteresis loop measurement, derived from the images. *Khela et al.* [48] applied wide-field Kerr microscopy to $CrGeTe_3$ material, demonstrating that perpendicularly magnetized band and bubble domains in *bulk*, one millimeter thick crystals can be generated and manipulated by ultrafast laser excitation.

We have chosen $Cr_2Ge_2Te_6$ (abbreviated as “CGT" in the following) exfoliated flakes for testing. CGT is a semiconducting material that belongs to the family of transition metal dichalcogenides layered materials, characterized by strong in-plane covalent bonds and weak interlayer van-der-Wals interactions [49]. Due to this layered atomic arrangement, thin and ultrathin (2D) films can be easily exfoliated from bulk crystals. Most relevant for this article is the fact that CGT has a ferromagnetic ground state below a (bulk) Curie temperature of 61 K and a high uniaxial magnetic anisotropy perpendicular to the atomistic layers, both, in bulk crystals as well as exfoliated flakes. Therefore all magnetic experiments on CGT material require cooling and the possibility to apply perpendicular magnetic fields.

Several domain studies in low-dimensional CGT crystals have been reported: *Han et al.* [25] used cryo-LTEM on 90 nm to 300 nm thick flakes and found band domains with a thickness-dependent width between 150 nm and 400 nm that transformed into skyrmionic bubble domains of about 100 nm diameter in applied perpendicular fields. Applying the same method, band domains and bubble lattices with sizes around 100 nm were later seen by *McCray et al.* [32] on 60 nm to 150 nm thick flakes and more recently by *Thomsen et al.* [34]. In the latter work it was shown that the bubble domains doubled their diameter from 90 nm to 180 nm when the crystal thickness was increased from 100 nm to 400 nm. It was further found that exposure to ambient conditions for five days resulted in a 5 nm thick surface oxide layer on the flakes that reduced their effective magnetic thickness thus having an influence on the domain width. Besides cryo-LTEM, also other imaging tools were used to study the domains in thin CGT crystals: *Powalla et al.* observed band domains with a width around 60 nm on 50 nm thick crystals by STXM [40], and patchy stray-field contrasts were seen by *Vervelaki et al.* [42] on 11 nm thick specimens by the mentioned microSQUID scanning microscopy (by micromagnetic simulations it was shown that those contrasts may arise from 50 nm wide band domains). The same method was previously applied by *Noah et al.* [41] on related $CrGeTe_3$ crystals, providing a thickness-dependent domain state diagram for that material. Again, irregular multidomain states with a patchy appearance were seen for flakes thicker than 10 nm, whereas a 6 nm thick flake was in a monodomain state at zero field, revealing wider patch domains during the magnetization process. *In summary*, perpendicularly magnetized band- and bubble domains with sizes in the 100 nm range have been observed on low-dimensional CGT crystals with thicknesses ranging between ten and several hundred nanometers. Wide-field MOKE microscopy was, to our best knowledge, not yet applied to image thin CGT crystals. By *laser-scanning* MOKE microscopy, however, domains have been seen in the

[3] In their article [18], the authors provide high-contrast domain images without scale bar in Figs. 2 and 4, whereas in the real MOKE micrographs in that paper domains are only weakly visible (except for the thickest crystal in Fig. 5). Although not explicitely mentioned in the article, the high-contrast domain images are supposed to be sketches [*Cheng Song*, private communication with the corresponding author]. Also the wide domains with irregular domain walls, claimed to be seen for the thinnest crystals, cannot be identified in the presented images

mentioned 1 mm thick $CrGeTe_2$ specimens [48], and this technique was also applied in the pioneering article of *Gong et al.* [1] to prove the existence of ferromagnetic order in 2D CGT crystals for the first time.

In this article we show that *cryo-wide-field Kerr microscopy* cannot resolve magnetic domains on low-dimensional CGT flakes due to (expected) domain sizes around 100 nm, which is well below the resolution limit in the 500 nm regime. Using a wide-field Kerr microscope in the magnetometer mode, however, turns out to be very useful to measure hysteresis loops on vdW flakes as it allows to precisely select particular areas of specific flake thicknesses, which would not be as easy possible in laser-based MOKE setups and not at all be possible by applying integral hysteresis techniques. We furthermore address the role of the compensator, showing that it is the decisive optical element in MOKE magnetometry and microscopy on ultrathin specimens as it allows to maximise the Kerr signal.

## II. EXPERIMENTAL

### A. SAMPLE PREPARATION

Single crystals of CGT, with approximate dimensions $5 \times 5 \times 0.2$ mm, were grown using the self-flux method as described elsewhere [50]–[52]. To get thin CGT flakes on 285 nm thick oxidized silicon wafer substrates, we used mechanical exfoliation with scotch-tape. The principle of mechanical exfoliation is based on the mentioned van der Waals forces along the c-axis, which are relatively weak thus allowing the layers to be mechanically separated [3]. By repeated exfoliation it is possible to obtain increasingly thin layers, potentially down to a few layers. These flakes were randomly distributed on the wafer′s surface and were then carefully checked under an optical microscope equipped with white light. The obtained flakes′ thicknesses ranged from hundreds of nanometers down to 4 nm, corresponding to two to three atomic layers.

Given that CGT is highly susceptible to rapid oxidation when exposed to atmospheric conditions [2], [34], the entire exfoliation process as well as the optical microscope investigation were conducted within an argon-filled glovebox. This controlled environment prevented exposure to air, maintaining the pristine state of the exfoliated flakes before the magneto-optical measurements were conducted. The flakes were finally transferred to the Kerr microscope using a sealed flow-cryostat loaded inside the glove-box, so that no air exposure could degrade the thin flakes. For comparison, an additional CGT flake was intentionally exposed to ambient air for several days to induce oxidation, allowing us to investigate the effects of prolonged air exposure on the material.

Due to the absence of an atomic force microscope (AFM) within our glove-box, the thickness of the investigated flakes was first roughly estimated from their color under the white-light optical microscope. At the nanometer thickness range, the flakes′ color arises from thickness-dependent light interference effects [2]. In the case of CGT, the color varies rapidly below 15 nm thickness (see Fig. 3 below), allowing a relatively precise thickness estimation of sub-15 nm thick flakes without AFM. After the Kerr microscopy investigations, the flakes were finally taken to air and their thickness was precisely determined using AFM.

### B. MOKE MAGNETOMETRY AND MICROSCOPY

The exfoliated CGT flakes have then been characterized by hysteresis measurement and domain observation, performed by MOKE magnetometry and microscopy, respectively. As the Curie temperature in CGT material depends on thickness, going down from 61 K (bulk) to 32 K when reaching the bilayer thickness [1], all relevant experiments have been performed at a temperature of 5 K (the lowest temperature we could achieve) to make sure that we are well in the ferromagnetic regime also for the thinnest flake areas. To estimate the Curie temperature of our material, a series of magnetization loops was measured at increasing temperature (see Supplementay Material), demonstrating that the magnetic response from the flakes vanishes between 50 and 55 K.

All magneto-optical studies were carried out in a wide-field Kerr microscope [53], equipped with a monochromatic CMOS camera and background subtraction for contrast enhancement [54]. The flakes were mounted in an optical flow cryostat that was operated with liquid helium. A solenoid was placed around the cryostat, allowing to apply magnetic fields perpendicular to the flake plane up to $\mu_0 H = 110$ mT. The Kerr contrast could be freely adjusted by opening the analyser and compensator on the reflection path of the polarization microscope by some degrees relative to the polarizer that creates plane-polarized light on the illumination path. The compensator, a quarter-wave plate in our case, was placed in front of the analyser. Perpendicular incidence of light, i.e. the polar Kerr effect was exclusively used. The measurements were performed with red or blue LED (Light Emitting Diode) light with wavelengths of 650 nm and 460 nm, respectively, or with white light. For a review on wide-field Kerr microscopy, including cryogenics, we refer to ref. [46]. The function and role of the compensator is reviewed in ref. [55].

In the cryostat, the silicon wafer substrate together with the CGT flake was mounted on a cold finger using silver paste and set under vacuum. Imaging was performed through an optical window between the objective lens and the sample. A long distance objective with a $60\times$ magnification and a numerical aperture of $NA = 0.6$, optically corrected for the glass window, was used. This restricts the achievable spatial resolution. Following the Abbe resolution criterion, the resolving power $R$ is expressed by $R = 0.5\lambda/NA$. It defines the smallest distance between two objects so that they can still be distinguished. For the used objective lens and for red light with $\lambda = 650$ nm, a spatial resolution of 540 nm is expected [46].

Our setup can be used for both, domain imaging as well as magneto-optical magnetometry. For the latter, a region of interest is selected in the domain image and then the Kerr intensity, integrated over all camera pixels in that region, is plotted as a function of applied magnetic field. Intensity

changes due to the magneto-optical Faraday effect, generated in the objective lens and glass window, can be technically corrected during the measurement [47]. The magnetization loops, presented in this work, have been measured "quasistatically", i.e. the magnetic field was changed in steps with a duration in the second range.

## III. THEORETICAL BACKGROUNDS

In this section we present some theoretical background of magnetic domains that is of relevance for this article, and we discuss the depth dependency of the magneto-optical Kerr signal. Both will then be used in Sect. V to discuss and interpret our experimentally obtained hysteresis and domain data, that are presented in Sect. IV.

### A. DOMAIN THEORY

As with any magnetic material, it is advisable to start the discussion of magnetic domains with the quality factor, $Q$, in order to classify the domains in our CGT flakes appropriately. This dimensionless material parameter reflects the interplay of anisotropy energy and stray field energy and thus determines the domain character [56]. It is defined as [57]

$$Q = K_\mathrm{u}/K_\mathrm{d} \ , \tag{1}$$

where $K_u$ is the uniaxial magnetocrystalline anisotropy constant, $K_\mathrm{d} = \frac{1}{2}\mu_0 M_\mathrm{s}^2$ is the stray field energy coefficient which is a measure for the maximum energy density that may be connected with stray fields, $M_s$ is the saturation magnetization and $\mu_0$ the vacuum permeability. Assuming the parameters for *bulk* CGT material, $M_s = 168\,\mathrm{kA/m}$ [40] and $K_u = 47\,\mathrm{kJ/m^3}$ [50], the quality factor [57] of our material is calculated as $Q \approx 2.7$ with $K_\mathrm{d} = 17.7\,\mathrm{kJ/m^3}$. With $Q > 1$ and the anisotropy axis perpendicular to the surface of the exfoliated flakes, we can expect band domain patterns [57] in the ground state, i.e. up-and-down magnetized domains as sketched in Fig. 1 (often called "stripe domains" in the literature). They can be arranged in a maze or parallel pattern depending on the magnetic field history. Closure domains at the surfaces will not occur — they would be favourable to (further) reduce the stray field energy, but their magnetization would deviate from the anisotropy axis which is prohibited by the dominating anisotropy.

A domain theory for magnetic films with perpendicular anisotropy, including closure domain models for $Q \ll 1$ materials as well as band domains for $Q \gg 1$ materials, was first presented by *Kittel* [58], based on the minimization of the total energy that comprises anisotropy energy, domain wall energy, and stray field energy. In case of band domains, being strictly magnetized along the anisotropy axis, the equilibrium domain width is determined by the competition between stray field energy and domain wall energy: the former is reduced by domain formation thus favouring the finest possible domains, whereas the wall energy is lower for wide domains, i.e. fewer domain walls. Kittel found that for any $Q$-value the basic domain width decreases proportionally to the square root of the film thickness. *Málek* and *Kamberský* [59] have then refined the Kittel model for band domains, rendering the demagnetizing energy more accurately by taking into account flux closure not only between the band domains but also inside the film. Shortly afterwards, *Kooy* and *Enz* [60] have extended the model by adding the external magnetic field energy thus being able to calculate magnetization curves. They have furthermore improved the model by incorporating the so-called $\mu^\star$-correction [57] in the calculations, which allows some tilting of the magnetization away from the perpendicular easy axis when approaching the film surfaces to further lower the stray-field energy, thus extending the band domain model towards lower $Q$. It turns out that for $Q > 0.8$ the $\mu^\star$-corrected band domain model offers the best estimate for uniaxial films, whereas for $Q \gg 1$ the $\mu^\star$-correction can be neglected (according to $\mu^\star = 1 + 1/Q$). For materials with $Q < 0.8$ different domain models with some kind of flux closure domains do apply [57].

In this article we are just interested in an *order-of-magnitude* estimation of the band domain width to assess the extent to which MOKE microscopy can resolve the domains. We therefore neglect the $\mu^\star$-correction for simplicity, assuming band domains that are strictly magnetized along the perpendicular easy axis all through the film. For our estimation we furthermore assume that both, anisotropy and domain wall energy are independent of the flake thickness[4]. We follow the *Kooy and Enz* [57], [60] treatment, which is based on the minimization of the total energy in an infinitely extended film comprising the stray field energy of the domain configuration, the domain wall energy, and the applied perpendicular field energy. To express the competition between gain in stray field energy and expense of domain wall energy, a *characteristic thickness*,

$$d_\mathrm{c} = \gamma_\mathrm{w}/2K_\mathrm{d} \ , \tag{2}$$

is introduced [57] with $\gamma_\mathrm{w} = 4\sqrt{AK_\mathrm{u}}$ being the specific domain wall energy of the (assumed) 180° Bloch walls and $A$ the exchange stiffness constant. If the film thickness is below $d_\mathrm{c}$, equilibrium band domain patterns will hardly be formed in the film: the gain in stray field energy through domain formation becomes negligible then and the formation of equilibrium domains will be suppressed by any trace of wall coercivity. Note, however, that domains in an infinitely extended film can nevertheless *exist* even if it is thinner than the characteristic thickness — at zero field, there can always be a perpendicularly magnetized domain state with a domain size that varies between narrow band domains and macroscopic domains depending on the size of the quality factor $Q$ [63]. *Equilibrium* domains, however, can hardly be formed in ultrathin films when wall pinning effects play a role. In such ultrathin films, domains are especially expected to be formed during the magnetization process. For cobalt films with thicknesses in the few-monolayer regime and a

[4] Ab-initio density functional calculations have predicted that CGT should have a decreasing anisotropy with decreasing film thickness and that an in-plane anisotropy can be expected when approachng the monolayer regime [61], [62]

perpendicular anisotropy that is caused by surface anisotropy, for instance, it was found that the nucleation and growth of irregular, patchy perpendicular domains dominates the magnetization process [64].

Some calculated equilibrium magnetization curves, taken from Fig. 3.113 in ref. [57], are plotted in Fig. 1(a). Parameter is the characteristic thickness $d_c$, but now reduced by the film thickness $D$, i.e. $\lambda_c = d_c/D$. The magnetization $m = (W_1 - W_2)/(W_1 + W_2)$ is defined in terms of the widths of the domains magnetized along ($W_1$) and opposite ($W_2$) to the direction of the applied field. The magnetic field is given by $h = H/M_s$, i.e. the applied field $H$ is reduced by the saturation magnetization $M_s$ that corresponds to the demagnetizing field $H_d = -NM_s$ of a film homogeneously magnetized out-of-plane with the demagnetizing factor $N = 1$. From the plots in Fig. 1(a) it is obvious that in the limit of large thicknesses (small $\lambda_c$) the magnetization curve approaches the line $m = h$ as expected for a thick film in perpendicular field when the contribution of the domain wall energy can be ignored [57]. When $\lambda_c$ increases, saturation is reached in fields considerably smaller than the demagnetizing field and the initial slope of the curves rises. This indicates an increasing influence of the domain wall energy with decreasing thickness, making domain states increasingly unstable. Furthermore, the magnetization curves are not straight lines anymore but show characteristic deviations with an increasing slope on approaching saturation. Here the domain period, $W_1 + W_2$, diverges and the domain width $W_2$ of the minority domains approaches a constant value, increasing their mutual distance with raising field till they finally disappear at saturation [57], [60]. In the *Kooy and Enz theory* another phenomenon, which is often observed when the applied field exceeds some critical value, was not considered: the transition of band domains to a *bubble domain lattice* that is energetically more favourable with increasing field (note that bubble lattices may also exist as metastable configurations at the same field levels as band domains). Such transitions do not change the principle magnetizaion curve character, though [57].

Finally, let us point out that 2D vdW materials are in fact a novel material class that deserves attention due to their distinctive electronic, optical and magnetic properties [3]. Research on the magnetism of (general) 2D materials with perpendicular anisotropy, especially on their domain structure, however, has already a much longer history. It has started more than 60 years ago with the mentioned works by *Málek and Kambersk*ý [59] and *Kooy and Enz* [60], which were related to magnetic storage media and in which the critical thickness $d_c$ was identified below which 2D films are expected to be free of equilibrium domains. About 30 years later the magnetism of ultrathin films raised research interest again after the discovery of ferromagnetic-antiferromagnetic oscillations in exchange coupling and the giant magnetoresistance effect in magnetic multilayers, which have gone hand in hand with the preparation of high-quality epitaxial films. Symmetry breaking at interfaces and surfaces may cause perpendicular anisotropies in such high-quality ultra-

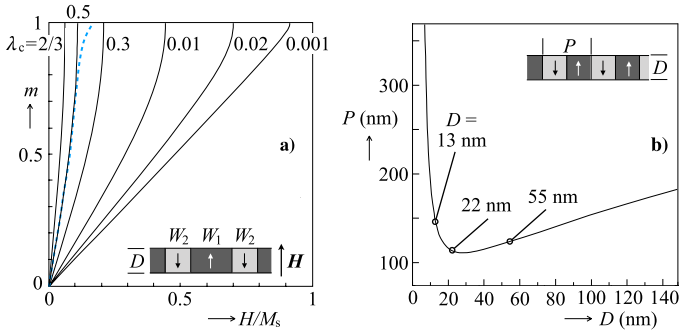


**FIGURE 1. (a) Equiibrium magnetization curves (in bold) of arbitrary thin films with perpendicular anisotropy as a function of an applied magnetic field perpendicular to the surface, calculated for the band domain model according to the *Kooy* and *Enz* [60] theory and given in reduced units (the curves are adapted from Fig. 3.113 in ref. [57]). The parameter $\lambda_c$ is the ratio between the characteristic thickness $d_c$ and the film thickness, see text. In *dashed* the measured curve for our 13 nm thick CGT crystal from Fig. 6(c) is added – plotted is the average of the two ascending branches. (b) Band domain period *P* as a function of film thickness *D* for our CGT films, adapted from Fig. 3.114b in ref. [57] by assuming the measured characteristic thickness of $d_c$ = 7.4. Three thickness values are highlighted, showing that domain periods in the range between approx. 110 nm and 150 nm can be expected for typical CGT flakes**

thin films, leading to unexpected domain effects as reviewed by *Allenspach* [64].

### B. DEPTH DEPENDENCY OF THE KERR SIGNAL

In Sect. IV we will show that the Kerr signal in the magneto-optically measured hysteresis loops on CGT flakes strongly depends on the flake thickness and that even its sign may be inverted for different thicknesses under the same experimental conditions. We will furthermore see that an inversion of the Kerr signal is also possible by changing the wavelength of the light.

To understand those observations, we need to consider that the Kerr effect is *not* a "surface" effect. For metallic materials we can rather expect a *information depth* of the order of the skin penetration depth, i.e. of some ten nanometers typically [65]. For a quantification of this depth sensitivity, it needs to be taken into account that for the Kerr effect the specimen is illuminated with plane-polarized light, which is then rotated and possibly elliptically polarized on reflection [46]. The reflected light may actually be seen as being composed of two components: a magnetically unaffected, primary light field called normally reflected amplitude, $A_N$, that is polarized along the same plane as the incoming light and that is governed by the Fresnel reflection coefficients, and a much smaller, magnetically induced contribution called Kerr amplitude, $A_K$, which is polarized perpendicular to $A_N$ in case of the longitudinal and polar Kerr effects. Interference of $A_N$ and $A_K$ will lead to pure Kerr rotation if both are in-phase and to elliptical polarization if they are out-of-phase. Both, Kerr rotation and ellipticity depend on the magnetization direction in the specimen and a Kerr contrast is obtained by converting them to a magnetization-dependend signal by means of an

analyser and compensator[5]. A compensator [55] is a phase shifter like a quarter wave plate, placed in front of the analyser in the Kerr microscope. By rotation around the propagation axis it allows to select the phase difference between $A_K$ and $A_N$ freely so that ellipticity can eventually be eliminated (i.e. compensated). This is helpful to obtain a detectable Kerr signal as plane-polarized waves can be better converted to a contrast by the analyser.

The phase of the Kerr amplitude is also the key to quantify the depth sensitivity of the Kerr signal. Here one has to consider that in case of metallic materials the amplitude of the light wave, entering the material, is exponentially damped and increasingly shifted in phase with increasing depth. At each depth it generates a Kerr amplitude as schematically indicated in the inset of Fig. 2a, which has to travel back to the surface, thus being absorbed and phase-shifted again by the same amount. The phase difference of the Kerr amplitudes is taken into account by the phase factor or complex penetration function [55], [65], [67]

$$\varphi(z) = \exp(-\eta z) \text{ with } \eta = \frac{2\pi}{\lambda_0}\, \mathrm{i} \cos\vartheta_1\, n_1\,. \qquad (3)$$

Here $z$ is the coordinate perpendicular to the surface, $\lambda_0$ is the (vacuum) wavelength of the illuminating light, and $\vartheta_1$ the angle of light incidence *within* the specimen. This phase factor also comprises absorption by using a complex refractive index $n_1 = n_1' - \mathrm{i}n_1''$ in case of a metallic specimen. For a thorough review of the role of the phase factor for the description of the depth sensitivity in magneto-optics we refer to ref. [55][6].

Here we restrict the discussion to the *polar Kerr effect* as it was also used in the experiments. Assuming perpendicular incidence of light and a homogeneous, perpendicular magnetization, the depth sensitivity function of the Kerr amplitude for a *bulk* specimen is written as [67]:

$$s^{\mathrm{pol}}_{\mathrm{bulk}}(z) = K^{\mathrm{pol}}\, 2\, \eta_{\mathrm{perp}}\, \varphi(2z)\ , \qquad (4)$$

$$\text{with } \eta_{\mathrm{perp}} = \frac{2\pi}{\lambda_0}\, \mathrm{i}\, n_1 \text{ and } K^{\mathrm{pol}} = \frac{iQ_{\mathrm{V}} n_1}{4n_0}\, t_{01}^2\,.$$

The coefficient of the polar Kerr effect, $K^{\mathrm{pol}}$, contains the first-order Voigt parameter $Q_{\mathrm{V}}$ (a material parameter describing the strength of the Kerr effect), the refractive index $n_0$ of the medium "0" from which the light enters the sample, and the Fresnel transmission coefficient, $t_{01}$, describing the transmission of light from medium "0" to the specimen with index "1". The factor 2 reflects the fact that the light wave must travel in and out to lead to an emerging Kerr amplitude.

For illustration, the real- and imaginary parts of the complex sensitivity function (4) are plotted by bold lines in Fig. 2a for a bulk $Cr_2Ge_2Te_6$ crystal. Both curves resemble simple, damped oscillations that are shifted in phase. For the figure, the sensitivity function was normalized to the function right at the surface, i.e. plotted are the real- and imaginary parts of $\kappa = s^{\mathrm{pol}}_{\mathrm{bulk}}(z)/s^{\mathrm{pol}}_{\mathrm{bulk}}(z=0)$. This eliminates the prefactors $K^{\mathrm{pol}}$ and $\eta_{\mathrm{perp}}$ in (4) as they do not depend on $z$ so that only the wavelength, $\lambda_0$, and the refractive index of the material, $n_1$, enter the function. The latter was taken from ref. [68], whereas the Voigt parameter, which seems not to be known for CGT material, does not play a role anyway in this representation. The total *effective* Kerr amplitude, which finally interferes with the effective regular amplitude, can be seen as a superposition of the phase-shifted contributions from different depths and is obtained by integrating the depth sensitivity function (4) as illustrated in Fig. 2b.

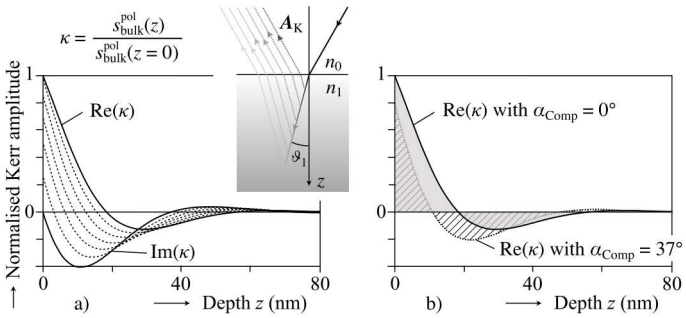


**FIGURE 2. (a) Depth dependence of the polar Kerr amplitude for bulk $Cr_2Ge_2Te_6$ material, normalised to the Kerr amplitude at the surface with $n = 3.12 - i\,2.31$ and $\lambda_0 = 460$ nm. Perpendicular magnetisation and perpendicular incidence of light was assumed. For the dashed curves between the real- and imaginary part graphs the phase of the Kerr amplitude was shifted in steps of 15 degrees. The inset illustrates the partial beams that are contributing to the Kerr amplitude, but shown for oblique incidence. (b) Integration of the sensitivity curve leads to the total Kerr amplitude, shown here for the real part curve in (a), i.e. for maximum surface sensitivity, and a phase-shifted curve (dashed) for which the total Kerr amplitude is eliminated.**

Due to the normalization, the real-part curve in Fig. 2a represents a Kerr sensitivity for which the Kerr amplitude generated right at the surface is in-phase with the normally reflected amplitude so that the surface magnetization is detected optimally. At a certain depth, where the sensitivity passes zero, the magnetization will be invisible and magnetization contributions deeper in the material will even reduce the overall Kerr signal. In practise, the relative phase of the Kerr- and normally reflected amplitudes is adjusted by means of the compensator, which allows to freely select any phase difference between the two amplitudes by rotating it around the axis of light propagation as mentioned. This means that any linear combination between the real- and the imaginary part of the Kerr amplitude can be realised by proper compensator settings. If, for instance, the phase sensitivity is shifted by 90° compared to the phase of the surface amplitude, the imaginary part curve in the Fig. 2a will become the real part curve. As this curve starts at zero there is no sensitivity to the magnetization right at the surface and only the subsurface magnetization will contribute to the Kerr signal. In the figure some linear combinations are plotted by dashed lines. They are obtained

[5]Note that a Kerr signal can also be obtained without analyser and compensator by making use of unconventional magneto-optical effects, see ref. [66] for a review

[6]If the reader wants to verify the equations given here by comparison with ref. [55], we ask to be aware of misprints in that book: In equation (2.92a) the nominator of the first fraction must read $n_1 \cos\vartheta_0 - n_0 \cos\vartheta_1$, and in equation (2.92d) the fraction must be positive. In the third term of equation (2.85), $r_{yy}$ must be replaced by $r_{yx}$. Furthermore, in equation (2.97a) the minus sign in the third vector component has to go to the second component.

by $s^{\mathrm{pol}}_{\mathrm{bulk}}(z) = \cos(\alpha_{\mathrm{Comp}})\mathrm{Re}(\kappa) + \sin(\alpha_{\mathrm{Comp}})\mathrm{Im}(\kappa)$, with $\alpha_{\mathrm{Comp}}$ being the phase shift of the Kerr amplitude counted from the real part curve and changed in steps of 15° in Fig. 2a. If a quarter wave plate is used as compensator, $\alpha_{\mathrm{Comp}}$ would be equal to the "opening angle" of the compensator — zero opening (i.e. compensator not active or absent) would result in the plotted real part curve and rotation by 90° would cause a phase shift of 90° so that the imaginary part curve becomes real. Besides the real-part curve, which reveals a positive Kerr amplitude after integration, Fig. 2b also shows the sensitivity curve for a vanishing Kerr signal at a compensator setting of $\alpha_{\mathrm{Comp}} = 37°$.

Whereas in bulk material only the Kerr amplitude and its interference with the regular amplitude has to be considered to describe the magneto-optical depth sensitivity, in case of magnetic films with a thickness below the penetration depth also the *Faraday* effect has to be taken into account, i.e. transmitted magneto-optical beams need to be considered. Together with the regular beam, they are multiply reflected at both surfaces of the film thus creating new Kerr amplitudes within the film, so that the depth sensitivity function of the whole film is finally obtained by summation of all those elementary rays[7]. For the polar Kerr effect, the sensitivity function of a magnetic film can then explicitly be written as [55], [67]:

$$s^{\mathrm{pol}}_{\mathrm{film}}(z) = K^{\mathrm{pol}}\, 2\, \eta_{\mathrm{perp}} \frac{\left[\varphi(z) + r^{12}\varphi(2D - z)\right]^2}{\left[1 - r^{10} r^{12} \varphi(2D)\right]^2} \,. \qquad (5)$$

Here $r^{ik} = (n_i - n_k)/(n_i + n_k)$ are the Fresnel amplitude reflection coefficients describing the reflection of light from medium "1" to medium "k" with medium "1" being the magnetic film. The light enters the film from medium "0" and medium "2" is on the backside. For $D \to \infty$, equation (5) yields the same results as the bulk sensitivity function (4).

In Sect. V-D we will apply (5) to calculate exemplary sensitivity functions for CGT films with different thicknesses and light colour to demonstrate the role of the compensator in magneto-optical experiments on ultrathin films.

## IV. HYSTERESIS MEASUREMENTS AND DOMAIN OBSERVATIONS

In Fig. 3 we demonstrate that magnetic hysteresis loops on perpendicularly magnetised CGT flakes can well be measured in a wide-field Kerr microscope. The relative settings of analyser and compensator were *intuitively* adapted to obtain a good polar Kerr signal on a given flake and then the loops were measured with the same settings. On our specimens it turned out that red light gave the best Kerr contrast compared to white and blue light (not shown).

Whereas for 7.8 nm thickness a highly-coercive, very noisy hysteresis loop was measured, no Kerr signal could be obtained at a flake thickness of 4 nm. Above 9 nm thickness, however, clear loops could be measured that change their character with increasing thickness from open (9 nm) to "pinched" shapes with shoulders on the descending branches (12 nm and 13.5 nm), indicating that a delayed and rapid change in magnetization takes place at the beginning of the reversal process. All loops are sheared, owed to the demagnetization effect of such thin film specimens in perpendicular field. At first glance, it may seem surprising that the shearing increases with increasing flake thickness. Note that the flake for Fig. 3 was exposed to air for several days between exfoliation and magneto-optical imaging.

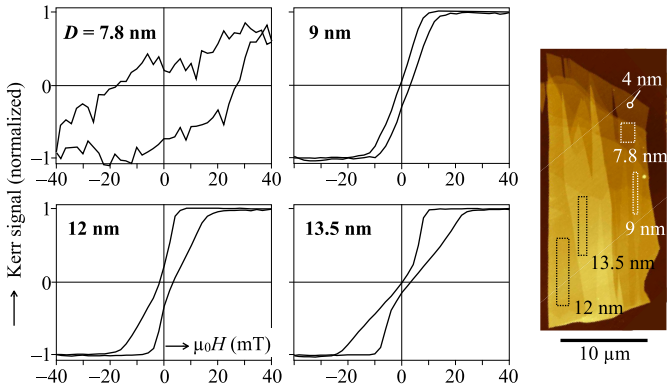


**FIGURE 3. Hysteresis loops of a $Cr_2Ge_2Te_6$ (CGT) flake, measured in perpendicular magnetic field under polar Kerr conditions in regions of different thickness *D* as indicated. The frames in the AFM micrograph show the areas in which the loops have been obtained by plotting the averaged Kerr signal. All loops were measured at a temperature of 5 K and by using red light. Analyser and compensator have been intuitively adjusted for maximum Kerr signal. For each curve, the MOKE signal is normalized to the Kerr signals at bright (-1) and dark (+1) saturation. The image of the flake was taken in a normal optical microscope with a colour camera. Note that this flake was exposed to air after exfoliation**

The evolution of magnetic contrast along the reversal process of the flake in Fig. 3 is shown in Fig. 4(b), together with a topographic image in (c). That image was now obtained in the Kerr microscope, i.e. colours are lost due the applied monochromatic CMOS camera. Also the contrast is lower as compared to the AFM micrograph in Fig. 3. The topographic contrast was subtracted digitally from the live images during the field sweep to obtained the contrast-enhanced difference images in (b). In Fig. 4(a) the domains on the surface of a bulk CGT crystal are shown for comparison. Whereas "regular" domains are seen on the bulk crystal, the flake appears to be remagnetized by the growth of patchy areas with different grey levels in the regions of different thicknesses.

As mentioned, all data in Fig. 3 and Fig. 4 were obtained by using red light and specific, but fixed analyser/compensator settings that were intuitively chosen for each flake to maximise the average Kerr signal of the flake. For other settings unusual effects may be observed as presented in Figs. 5 and 6. Figure 5 shows the optical micrograph and a polar Kerr image obtained at magnetic saturation in a perpendicular field on a different flake sample. For the Kerr image the analyser/compensator setting was arbitrary, not optimized for maximum Kerr signal of the whole flake. Surprisingly,

[7] Such a Fresnel-type concept of multiple reflections and the interference of phase-shifted beams was also applied in ref. [68] to model the *optical* properties of 2D materials, calculating their wavelength-dependent reflection properties.

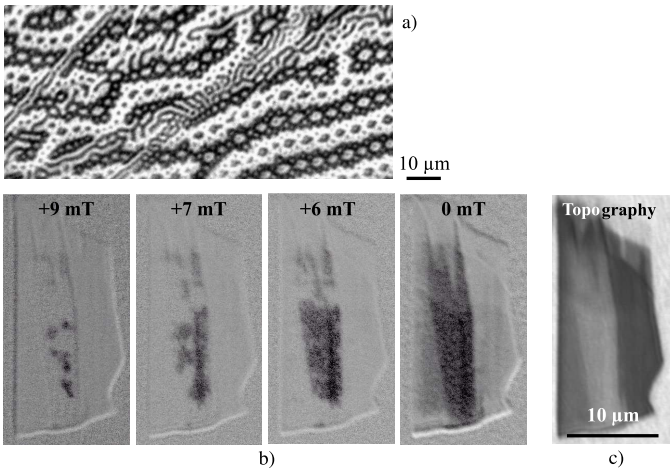


**FIGURE 4.** **(a) Typical domains on a CGT *bulk* crystal with a thickness of 0.2 mm, imaged on the surface perpendicular to the easy axis. Note the domain refinement along the scratches. (b) Domain evolution at a decreasing perpendicular magnetic field in the same flake as in Fig. 3, observed by polar Kerr microscopy. Image (c) shows the nonmagnetic (topographic) contrast as seen in the Kerr microscope. All domains were imaged at a temperature of 5 K and by using red light**

different regions of the flake show up in bright *or* dark rather than appearing in grey levels of one sign as one would expect [compare the series of images in Fig. 4(b), in which the whole flake switches from bright to dark]. Obviously the Kerr contrast is inverted for different layer thicknesses, leading to dark saturation for a thickness below 11 nm and a bright saturation for thicknesses above 13 nm. The inversion of the MOKE signal for different thicknesses of CGT flakes was already discovered by *Ma et al.* [12]. Those authors also found that the MOKE contrast can be inverted when choosing different wavelengths of light at a given thickness.

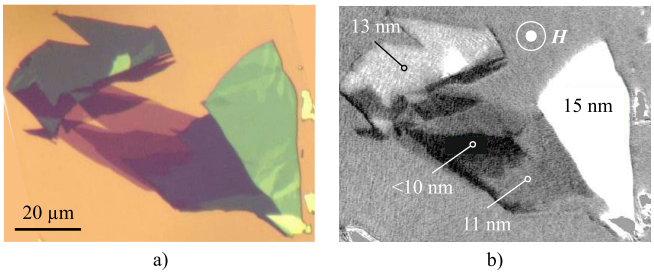


**FIGURE 5.** **Optical micrograph (a) and polar Kerr image (b) in a +50 mT perpendicular field of another CGT flake, measured under the same conditions as for the flake in Fig. 3 but for different compensator and analyser settings. A background image, taken at an applied field of −50 mT, was subtracted to obtain the Kerr difference image in (b). The thicknesses of some areas are indicated in (b)**

In Fig. 6 we have reproduced these effects on another CGT flake by presenting hysteresis loops at three thicknesses and two analyser/compensator settings, also adding the wavelength dependency of the Kerr signal. Whereas all three curves in Fig. 6(a), measured in blue light for some analyser/compensator setting, have the same sign, the curves for 13 nm and 22 nm thickness are inverted in (b) for another analyser/compensator setting. Fig. 6(c) shows the loops for the same analyser/compensator setting as in (a), but now measured in red light. Here the curves for 6 nm thickness change sign. By comparing all curves in the figure it is also evident that the noise level in the curves for red light is lower than for blue light, indicating that red light shows a stronger Kerr effect on CGT material. Noteworthy is also the mentioned increase in shearing (i.e. decrease of initial susceptibility) for increasing flake thickness, which is more pronounced here compared to Fig. 3 where a narrower thickness range is covered. Also note that unlike the flake for Fig. 3 and Fig. 4, the flakes for Figs. 5 and 6 were exfoliated and installed in the optical cryostat in a glovebox under argon inert gas atmosphere, thus avoiding exposure to air.

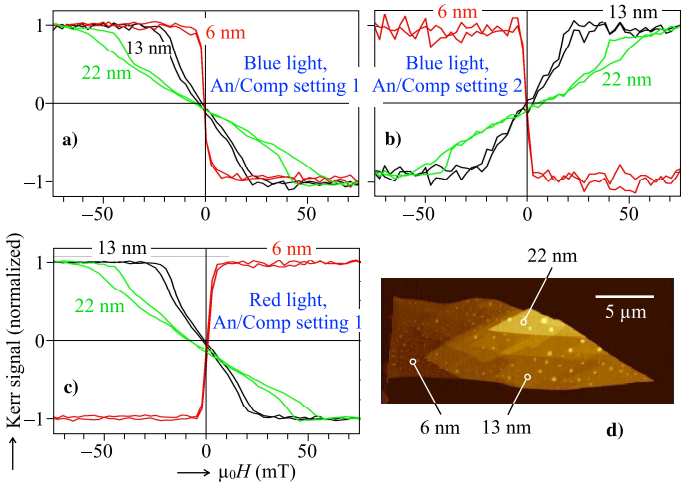


**FIGURE 6.** **Thickness and wavelength dependency of the Kerr signal, documented by polar MOKE magnetization loops on the CGT flake shown by the AFM image in (d). In figures (a) and (b) the loops were measured at different analyser/compensator settings in blue light, whereas figure (c) was measured in red light and with the same settings as in (a). Like in Fig. 3, the MOKE signal is normalized to its saturation value for each curve. Note that the analyser/compensator settings in this figure are not related to those in Fig. 3. Also note that for this figure the flake was protected from (severe) oxidation, different to the flake investigated in Figs. 3 and 4.**

## V. DISCUSSION

By the magnetometry and imaging experiments, presented in Sect. IV, we have shown that (i) in a wide-field Kerr microscope local hysteresis loops on exfoliated CGT flakes can well be measured, provided that some critical thickness is exceeded if the flake is exposed to air between exfoliation and imaging, indicating an influence of oxidation (compare the loops at 7.8 nm and 6 nm thickness in Fig. 3 and Fig. 6, respectively), (ii) all magnetization loops are sheared with an initial susceptibility that decreases with increasing flake thickness, (iii) for small thicknesses (9 nm for the flake in Fig. 3 and 6 nm for that in Fig. 6) regular (open) hysteresis loops are measured, whereas beyond those thicknesses the loops reveal a pinched character, (iv) the magnetization reversal of a flake seems to occur by the nucleation and growth of patchy areas rather than by "regular" domains, (v) the sign of the Kerr contrast may depend on the flake thickness and the light color used for the MOKE experiments, possibly

leading to a thickness- and wavelength-dependent inversion of the hysteresis loops for certain settings of analyser and compensator. In this section those experimental observations are discussed. First, we briefly summarize what can theoretically be expected for the magnetization curves and domains in our thin flake specimens with perpendicular anisotropy.

### A. EXPECTATIONS FROM THEORY

The calculated equilibrium magnetization curves in Fig. 1(a) have some similarity with the *ascending* branches of the measured pinched MOKE loops in Figs. 3 and 6. As an example, the curve measured for 13 nm thickness from Fig. 6(c) is properly normalized and added to the plots in Fig. 1(a) by taking the initial susceptibiiity (slope) of the measured curve as reference. Note, however, that a direct comparison between our measured and the calculated loops should be viewed with caution, since the measured curves are not equilibrium curves but rather determined by the magnetic field history along the curves including coercivity effects (and possibly domain wall creeping). This becomes most obvious when approaching saturation — here the measured curve in Fig. 1(a) significantly deviates from the the calculated curve (the even more pronounced shoulder-deviation along the descending branches is addressed in Sect. V-C). For a precise comparison, the curves should be measured in an anhysteretic (‘‘idealized") way [69] by superimposing ac magnetic fields of decreasing amplitude on every dc field step along the loop to wipe out the previous magnetic history. For our ‘‘order-of-magnitude" estimation of the domain width, however, only the initial susceptibility is relevant (see below) so that it is acceptable to work with our *quasistatically* measured loops.

Let us again choose the well-developed curve for 13 nm thickness in Fig. 6(c) as an example. Here the initial slope (or initial susceptibility) of the ascending branches, $\chi_{\rm in} = (\delta M/\delta H)_{M=0}$, has a value of approximately 7.4. Following *Gerritsma et al.* [70], the reduced characteristic thickness $\lambda_{\rm c}$ of the *Kooy and Enz* model can be determined from the initial susceptibility of the magnetization curves according to the following approximation:

$$\lambda_{\rm c} = \left(\frac{1 - 1/\chi_{\rm in}}{1.2}\right)^2 . \qquad (6)$$

With $\chi_{\rm in} = 7.4$ we get $\lambda_{\rm c} = 0.52$, and with the given thickness of 13 nm this results in a characteristic thickness of $d_{\rm c} = \lambda_{\rm c} D \approx 6.8$ nm. In case of the curve for 22 nm thickness in Fig. 6(c), the initial susceptibility is $\chi_{\rm in} = 3.6$, resulting in $\lambda_{\rm c} = 0.36$ and $d_{\rm c} \approx 8$ nm, thus being roughly of the same order as obtained for the 13 nm thick film. By taking the average for both thicknesses, let us assume a characteristic thickness of $\overline{d_{\rm c}} \approx 7.4$ nm for our CGT material in the following.

With that characteristic thickness we can now re-normalize the curve of Fig. 3.114b in ref. [57], in which the reduced domain periodicity, $P/d_{\rm c}$, is plotted as a function of the reduced thickness, $D/d_{\rm c}$, resulting in the curve shown in Fig. 1(b). It is obvious that with decreasing thickness the band domain period decreases, reaching a minimum of $P = 110$ nm at $D = 4d_{\rm c}$ (about 30 nm in our case), and than rapidly increasing again towards infinity. For films thinner than $d_{\rm c}$ a band domain pattern is not expected to form.

From (2) we can now also calculate the *specific domain wall energy*. For our CGT material, $\gamma_{\rm w} = 2K_{\rm d}d_{\rm c} \approx 2.7 \cdot 10^{-4}$ J/m$^2$ is found. This value is a bit below the range of $\gamma_{\rm w} = (4-7) \cdot 10^{-4}$ J/m$^2$ that was determined from domain observations on CGT flakes in ref. [34]. The authors have used cryo-LTEM to measure the band domain width as a function of crystal thickness. The curve in Fig. 1(b) could be (qualitatively) reproduced, but rather than finding a minimum domain period of $P = 110$ nm at $D = 30$ nm, as expected from Fig. 1(b), a minimum period of 160 nm was found in a broad thickness range between 60 nm and 120 nm. From that thickness range the authors of ref. [34] have derived the mentioned wall energy range using $D = 4d_{\rm c} = (4\gamma_{\rm w})/(\mu_0 M_{\rm s}^2)$. To explain the quantitative discrepancies one needs to consider that the LTEM measurements ref. [34] were not performed at zero field but rather in the presence of an 11 mT bias field that could not be avoided for technical reasons. Furthermore, it is not obvious if the sample was properly demagnetized, i.e. ‘‘idealized" as mentioned above to achieve the equilibrium domain period at zero field. Also stress effects, created by the preparation on TEM samples, may have an effect on the domain pattern via a sizable magnetostrictive term that was found for CGT material [32] and also mentioned in ref. [34]. The influence of mechanical stress can also be recognized by the domain refinement along the scratches in Fig. 4(a), again indicating the stress sensitivity of CGT material.

### B. DISCUSSION OF DOMAIN OBSERVATIONS

In Sect. III-A we have estimated a quality factor of $Q \approx 2.7$, indicating that in our CGT material the uniaxial, perpendicular anisotropy dominates over the stray field energy. This is confirmed by the 2-phase branched domain pattern [57], imaged on the surface of the bulk CGT crystal in Fig. 4(a). This pattern is similar to those observed on the basal plane of bulk NdFeB crystals with $Q \approx 4$, compare with Fig. 5.4 in ref. [57]. Branched domains like in Fig. 4a were also seen by magnetic force microscopy on a bulk CGT samples [10], [71] and on $Fe_3GeTe_2$ vdW crystals [72], [73].

Two-phase domain branching [57] is a phenomenon of thick crystals with $Q \gg 1$ and with a uniaxial anisotropy strongly misaligned to the main surface. It is characterized by a progressive domain refinement towards the surface by iterated generations of domains. The fine surface domains bring opposite magnetic poles in close distance, thus lowering the stray field energy, whereas the wide volume domains save domain wall energy. In the branching scheme, the basic volume domain width increases with the crystal thickness $D$ following a $D^{2/3}$ law. For $Q \gg 1$ materials with *perpendicular* uniaxial anisotropy, branching is expected [57] to occur beyond a characteristic thickness of $D_{\rm s} = \frac{1}{8}\pi^4 \gamma_{\rm w} F_{\rm i}^2 / C_{\rm s}^3$. Here $F_{\rm i} = \frac{1}{2}K_{\rm d}$ is a coefficient that considers internal stray fields connected to domain branching and $C_{\rm s} = 0.136 K_{\rm d}$

is the stray field energy coefficient at the surface. With the paramaters of our CGT material, $D_s$ is around 18 $\mu$m. Below that thickness, multiple-generation branching is expected to be replaced by un-branched band domains with undulated domain walls [74], and for thicknesses below the micrometer regime regular band domains with straight domain walls are preferred. In that regime the band domain width follows the mentioned $D^{1/2}$ law. When finally entering the thin film range, band domains with the thickness dependence shown in Fig. 1(b) are expected.

Whereas such branched domain patterns like in Fig. 4(a) are aesthetically appealing, this is unfortunately not true anymore for the patterns found by *Kerr microscopy* in the exfoliated flakes. In Fig. 4(b) the domain evolution in the same flake as for Fig. 3 is presented. As far as visible, the re-magnetization at each flake thickness starts by the nucleation and growth of patchy domains when the magnetic field is reduced from saturation. For our CGT flakes with a thickness above the characteristic thickness $d_c$ of about 7 nm and going up to 22 nm (the maximum thickness we have investigated) we actually *expect* band domains in the ground state with a period around 110-150 nm according to Fig. 1(b). In fact, such narrow domains have been seen on CGT flakes by cryo-LTEM [25], [32], [34], scanning SQUID-on-tip microscopy [42], and STXM [40]. In the latter article, band domains with a 130 nm periodicity at a flake thickness of 55 nm were observed which fits well to our calculated curve as indicated in Fig. 1(b). These authors also observed the mentioned increase of the distance of the minority domains and the appearance of bubbles when approaching saturation.

In our case, of course, such narrow domain widths are far below the lateral resolution of our cryo-Kerr microscope of about 540 nm (see Sect. II-B). The domain contrast in Fig. 4b may thus be seen as *integrated* contrast, which is actually caused by not-resolved band- and bubble domains. The presence of those domains in our specimens can indirectly be derived from the shoulder in the hysteresis loops, occurring for thicknesses above $d_c$, as discussed in Sect. V-C below. Although we cannot see the fine underlying domains, the patchy evolution of contrast indicates a locally varying domain nucleation across the whole flake, which could not be easily detected by Lorentz microscopy or other high-resolution techniques lacking the possibility of overview microscopy.

In this context, it is instructive to refer to the mentioned wide-field Kerr microscopy observations on the $Fe_3GeTe_2$ flakes performed by *Yin et al.* [18]. In that article the authors have seen faintly visible band domains in maze arrangement for a flake thickness of 32 nm. An estimate shows that their domain width at 32 nm thickness is indeed much closer to the optical resolution limit: In the supplementary material of ref. [18] a MOKE hysteresis loop is shown for a thickness of $D = 46$ nm that has an initial susceptibility $\chi_{in} = (\delta M/\delta H)_{M=0}$ of 9.8 along the ascending branch. Applying the routine developed in Sect. V-A, this results in $\lambda_c = 0.56$ (with $M_s = 376$ kA/m [34]) and a characteristic thickness of $d_c = \lambda_c D \approx 26$ nm. With that characteristic thickness and assuming the 32 nm thick flake, a reduced domain period of $P/d_c \approx 30$ can be derived from Fig. 3.114 in ref. [57], which corresponds to a domain period of almost 800 nm in real units, i.e. a domain width that is much closer to the resolution limit of cryo-MOKE microscopy (the actual resolution is not mentioned in ref. [18]). The *minimum* reduced domain period is expected to be at $P/d_c \approx 15$ according to Fig. 3.114 in ref. [57], which leads to a domain period $P$ of about 400 nm. So, even in case of $Fe_3GeTe_2$ material the finest possible domains would not be accessibel by Kerr microscopy.

Also interesting is the domain state for thicknesses below $d_c$, i.e. when the van-der-Walls flakes approach the real 2D limit. As discussed in Sect. V-A, an equilibrium band domain state is then not expected to exist anymore, whereas nonequilbrium domains can nevertheless exist and they will for sure be formed along the magnetization process. In the mentioned work by *Yin et al.* [18], the existence of a mono-domain state in $Fe_3GeTe_2$ flakes was in-fact verified by the measurement of square hysteresis loops for flake thicknesses below about 22 nm, which is below the critical thickness for that material. The authors claim to see wide domains during switching without showing evidence in their Kerr micrographs. On the other hand, irregular patch domain were seen in 6 nm thick $CrGeTe_3$ flakes by microSQUID scanning microscopy by *Noah et al.* [41]. In case of our CGT flakes we expect that they exist in multidomain states even if $D < d_c$. This is evident from the zero-remanence hysteresis curves shown for 9 nm thickness in Fig. 3 and for 6 nm thickness in Fig. 6. We will come back to that in Sect. V-C.

In summary, we *expect* that the pinched hysteresis loops, measured on our CGT flakes for larger thicknesses by polar MOKE magnetometry, are caused by the nucleation of regular band and bubble domains as they have been observed by LTEM and STXM. The final proof of this correlation would require a combined, in-situ loop measurement and domain observation, which is not possible with either Kerr or Lorentz microscopy — the former suffering from resolution and the latter from technical limitations in loop recording.

### C. DISCUSSION OF HYSTERESIS LOOPS

Having gained some understanding of the domains in the CGT flakes, as described in Sects. V-A and V-B, we can turn our attention to the hysteresis loops presented in Figs. 3 and 6.

Firstly, we note that at 7.8 nm flake thickness a highly-coercive and noisy loop was measured in Fig. 3 and that no Kerr signal was obtained at all for smaller film thicknesses. As the flake in Fig. 3 has been exposed to air, oxidation is the most obvious reason: an oxidised surface layer of several nanometer thickness may be assumed for that flake[8], leading to a complete oxidation of flake areas below this thickness

[8] As mentioned in the Introduction, *Thomsen et al.* [34] found that a 5-days exposure to ambient conditions resulted in an approximately 5 nm thick surface oxide layer on CGT material. Also note that non-oxidised CGT is known to display a Kerr signal down to the bilayer thickness [1]

range. For thicker areas, the effective *magnetic* flake thickness will be reduced by the thickness of the oxide layer. In fact, on our flake handled in the glovebox a well-defined loop could also be measured for a thickness of 6 nm (see Fig. 6), supporting this hypothesis. With a characteristic thickness $d_c$ of about 7 nm (Sect. V-A), below which band and bubble domains are highly unlikely, it is obvious that an open loop like that for $D = 6$ nm in Fig. 6 may be attributed to the absence of equilibrium domains during the magnetization process. The same conclusion can also be applied to the curve for $D = 9$ nm in Fig. 3 — if an oxide thickness of some nanometers is subtracted, the effective magnetic thickness will again be below $d_c$ thus resulting in an open loop. From a general comparison of the loops in Figs. 3 and 6 it is also obvious that the coercivities of the oxidised flake in Figs. 3 are higher than for the flake in 6, indicating that the formation of an oxide layer in low-dimensional vdW flakes has an influence on coercivity.

For thicknesses larger than $d_c$ we have shown in Sect. V-A that the ascending branches of the hysteresis loops of our CGT flakes resemble the magnetization curves obtained from band domain theory, at least up to about $m = 0.7$. When approaching saturation, the measured curves deviate from the calculated ones. This is all the more true for the descending loop branches, which are showing a shoulder or cliff in case of $D > d_c$. Such pinched hysteresis loops are well known for in-plane magnetized, low-anisotropy patterned elements made, e.g., of permalloy, for which the shoulder is caused by the retarded nucleation of a magnetization vortex at the sample edge [75] or by the sudden merging of edge domains [76]. Theoretically, such hysteresis effects close to saturation can be attributed to the topology of magnetic field penetration in case of in-plane magnetized films [77]. In media with perpendicular magnetic anisotropy (PMA), however, the appearance of shoulders in the magnetization curves is not considered in the band domain theory. Such shoulders in PMA films have first been measured in optically transparent, extended $BaFe_{12}O_{19}$ single crystal films with 3 $\mu$m thickness [60]. By Faraday microscopy it was shown that the plateau is related to the sudden nucleation of meander-shaped band domains. In those barium-iron-oxide films just a few nucleation centres were found to be active, and depending on the activated centre, the jump can occur at different fields. For both, in-plane and PMA media, the decisive criteria for the existence of shoulders is the elimination of all residual domains, i.e. true saturation, before the magnetic field is reduced. If this is not the case, straight loops without shoulder are measured.

Later such pinched loops were frequently measured also in various types of *sputtered*, i.e. polycrystalline PMA film media for perpendicular magnetic recording. For CoCr media [54] it was concluded that the better the crystallographic texture of the columnar grains, the more pronounced the shoulder is. For Co/Pt multilayers [78] it was found by domain observation that the magnetization jump was dominated by the avalanche-like propagation of one-dimensional band domains that originated from earlier nucleated bubble domains and that grew by domain wall motion. Depending on the number of residual domains left before decreasing the field, the avalanching was more or less suppressed and a more gradual rather than sudden domain growth was observed. In refs. [79], [80] it was shown by simulations that the degree of *structural disorder* dominates the reversal process in PMA media: strong disorder leads to a high density of nucleated domains that remain pinned by the structural disorder, thus needing a further decrease of the field to be able to grow and leading to smoothed or even suppressed cliff in the magnetization curve. Little disorder, on the other hand, leads to few nucleation centres, the avalanched growth of domains and well pronounced cliffs. These simulations are in agreement with experimental observations on CoPt multilayer films [81] for which the structural disorder was attributed to film roughness, controlled by the sputter pressure. In ref. [82] the reversal of FePt single- and FePd/FePt bilayer PMA films was compared. Pure FePt films showed pinched loops with the magnetization jump being caused by the avalanche growth of irregular band domains as expected. In the bilayers, an increased surface roughness together with spin canting in the FePd layer due to reduced perpendicular anisotropy compared to FePt favoured reversal by bubble domain nucleation, the density of which increases with decreasing field. A regular loop without shoulder was measured in that case.

Applying these findings to our single crystalline CGT flakes, a number of conclusions can be drawn: (i) Although we are unable to resolve the band or bubble domain patterns in our CGT flakes, it is very likely that the presence of a shoulder in a hysteresis curve is indirect evidence for the delayed nucleation of such domains, as has been demonstrated in numerous other PMA systems. (ii) A different degree of disorder and thus nucleation sides, which is used to explain the presence or absence of shoulders in the hysteresis loops due to the grain structure of sputtered films, can be excluded for our single-crystalline material. Our applied magnetic fields seem also to be strong enough to completely saturate the flakes during loop measurement thus eliminating residual domain nuclei. The obvious reason for the absence of the shoulder in the thinner CGT flakes is indeed the mentioned fact that $D < d_c$ and that the nucleation of band and bubble domains is not expected anymore. Nevertheless, from the zero remanence in the hysteresis curves of our thin flakes (9 nm and 6 nm in Figs. 3 and 6, respectively) it is expected that they exist in multidomain states at zero field, presumably similar to the nonequilibrium patch domains that were seen on $CrGeTe_3$ flakes by *Noah et al.* [41]. In our Kerr micrographs we could not identify the occurrence of such domains along the magnetization process, most likely owed to the fact that the areas of constant thickness in our flakes had extension of just some micrometers. (iii) Partial oxidation of the flakes may act similar to structural disorder in sputtered films, i.e. it may have an influence on domain nucleation and thus on the extend of the shoulder (besides affecting coercivity).

### D. ROLE OF THE COMPENSATOR

In Fig. 6 we have shown that the Kerr signal in the magneto-optically measured hysteresis loops strongly depends on the flake thickness and that its sign can even be inverted for different thicknesses under the same experimental conditions. As in MOKE magnetometry on bulk metallic specimens such effects are not observed, we may conclude that they are obviously related to the low thickness of the flakes. It was furthermore found that an inversion of the Kerr signal is also possible by changing the wavelength of the light.

These observations can be understood with the help of the depth-sensitivity concept of the Kerr effect presented in Sect. III-B. In Fig. 7 typical sensitivity functions according to (5) are compared for CGT films. Air was assumed on both sides of the magnetic film, i.e. $n_0 = n_2 = 1$[9]. Like in Fig. 2, the curves are normalized to the surface sensitivity so that the prefactors in (4) are eliminated and only the term with the phase factors is left. Plotted are curves for various compensator settings: In Fig. 7(a) and (b) two curves are shown for the same compensator setting, but for different film thicknesses. It is evident that for the given compensator angle the integral changes sign for the two thicknesses thus resembling the experimental observation in Fig. 6. In Fig. 7(c) and (d) the compensator setting and the film thickness are identical for both curves but the wavelength of the light was changed from blue to red. Again the integral changes sign thus resembling the experimental observation in Fig. 6.

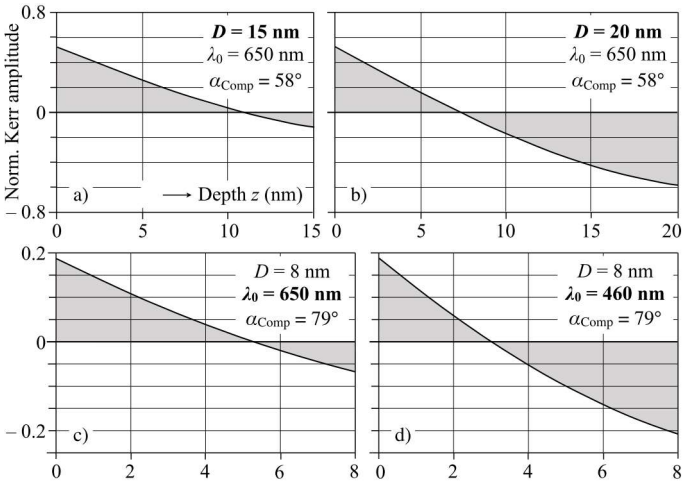


**FIGURE 7. Depth dependence of the polar Kerr amplitude for $Cr_2Ge_2Te_6$ *films*, normalised to the Kerr amplitude at the surface. Figures (a) and (b) have been calculated for the same compensator setting and wavelength, but for different film thicknesses as indicated. The integral and thus the Kerr signal has different signs for both thicknesses. In (c, d) the thickness and compensator settings were kept constant, but the colour of the light was changed from red to blue. Again the integral Kerr amplitude changes sign. The refractive indices, taken from ref. [68], are $n_1 = 3.78 - i\,2.08$ for $\lambda_0 = 650$ nm and $n_1 = 3.12 - i\,2.31$ for $\lambda_0 = 460$ nm.**

In summary, we have demonstrated that the experimentally-found sign inversion of the Kerr signal for different flake thicknesses and light colours can be explained on base of the magneto-optical depth sensitivity concept. Accordingly, the Kerr contrast is governed by the relative phase of the Kerr amplitude that can be freely adjusted by a rotatable compensator. A thickness-dependent Voigt parameter $Q_V$, like discussed in ref. [83], is not required to explain the thickness dependence of the Kerr signal. The compensator is thus the decisive optical element in MOKE magnetometry and microscopy on magnetic materials, including thin films and 2D vdW materials. It needs to be appropriately aligned to avoid a cancelation of the Kerr contrast and to maximise the Kerr signal. In practise this is done intuitively by rotating analyser and compensator simultaneously till the best signal is obtained. Of course, in case of exfoliated vdW flakes, which naturally consist of areas with different thicknesses, an optimization of the Kerr signal for one thickness may not be true for other thickness, so there exists no optimum analyser/compensator setting for the whole flake and the best chosen setting will be a tradeoff. This optimization must be carried out individually for each specimen — the settings for one sample cannot necessarily be transferred to another, as oxide layers of different thicknesses, for example, can also have an influence on the optimum settings in each case.

Finally note that in principle the Kerr sensitivity function could also be used to calculate the optimum compensator settings. However, this would require knowledge of the (bulk) Voigt parameter $Q_V$. Then the absolute, not normalized sensitivity function could be calculated and the proper compensator angle for maximum integral sensitivity could be determined. As $Q_V$ is not known for $Cr_2Ge_2Te_6$ material, no attempt is made in this article to perform such calculations. The calculations in this article are therefore intended only to prove the concept. For details on this depth sensitivity concept we refer to the mentioned review in [55] and to a series of articles in which it was developed [65], [67], [84]–[87].

## VI. CONCLUSIONS

We used a wide-field magneto-optical Kerr effect (MOKE) microscope to explore the potential of this method for the study of van-der-Waals (vdW) flake samples, utilizing its imaging- and hysteresis measurement capabilities and choosing exfoliated $Cr_2Ge_2Te_6$ (CGT) flakes as test samples. Due to the perpendicular anisotropy of such specimens and a ferromagnetic transition temperature well below room temperature, all experiments were carried out at a temperature of 5 K under the conditions of the polar Kerr effect and by applying magnetic fields perpendicular to the flake plane.

With the help of arguments from domain theory, we could show that in CGT flakes perpendicularly magnetized band domain patterns (and bubble domains in applied fields) with widths in the 100 nm range are expected, which in fact have been seen in the literature by high-resolution observations using Lorentz-electron microscopy and x-ray based imaging tools. Such domains could not be seen in our cryo-Kerr microscope due to insufficient resolution. However, their existence can be indirectly derived from shoulders in the hysteresis

[9] By selecting proper values for $n_0$ and $n_2$, any caping layer and substrate can easily be considered in our model — for simplicity, we have chosen air on both sides of the magnetic film, which is sufficient for the prove of concept

loops when deceasing the field from saturation. The band domain pattern is the zero-field ground state for CGT flake thicknesses above approx. 7 nm. This critical thickness was determined from the initial susceptibility of the recorded hysteresis loops. Below that thickness, equilibrium band domains are not expected to exist, which can be deduced indirectly from the disappearance of the shoulder in the hysteresis loops. From the critical thickness a specific domain wall energy of about $2.7 \cdot 10^{-4}$ J/m$^2$ for CGT flakes could be estimated.

We have furthermore demonstrated that the experimentally-found sign inversion of the Kerr signal for different flake thicknesses and light colours can be explained on base of the magneto-optical depth sensitivity concept. Accordingly, the Kerr contrast is governed by the relative phase of the Kerr amplitude that can be freely adjusted by a rotatable compensator. A thickness-dependent Voigt parameter $Q_\mathrm{V}$ is not required to explain the thickness dependence of the Kerr signal. The compensator is thus the decisive optical element in MOKE magnetometry and microscopy on magnetic materials, including thin films and 2D vdW materials. It needs to be appropriately aligned to avoid a cancelation of the Kerr contrast and to maximise the Kerr signal.

In general, MOKE magnetometry may be seen as method of choice to measure hysteresis loops on exfoliated, magnetic 2D vdW flakes as it allows to select flake areas with specific thicknesses, which would not be possible by integral hysteresis techniques. This areal selection is especially easy if MOKE magnetometry is performed in a wide-field Kerr microscope by plotting the image intensity as a function of magnetic field. By choosing a proper objective lens, the loops of a whole flake or at least large parts of it can be recorded in one step, later selecting an area of specific thickness in some post-treatment software in the computer and plotting the local loops. At the same time, the images provide information about the progress of the magnetization process and the domains supporting the process if they have widths above the resolution limit. Both is not easily possible in a laser-based MOKE magnetometer.

Independent of the imaging method used, we recommend to *idealize* the flake samples in future experiments, i.e. demagnetize them carefully by applying an ac magnetic field of decreasing amplitude. This allows to get to (or closer to) the domain ground state so that the equilibrium domain widths can be determined more reliably. The areas of constant thickness should be sufficiently large so that the domains can also form in their equilibrium state. This idealization procedure is also recommended for any kind of magnetometry used on vdW flakes. The obtained *anhysteretic* magnetization loops can be directly compared with the loops obtained from theoretical calculations, also allowing a more precise determination of the initial susceptibility from which the critical thickness and domain wall energy can be experimentally derived.

## REFERENCES


[1] C. Gong, L. Li, Z. Li *et al.*, "Discovery of intrinsic ferromagnetism in two-dimensional van der Waals crystals," *Nature*, vol. 546, pp. 265–269, 2017. [Online]. Available: https://doi.org/10.1038/nature22060

[2] B. Huang, G. Clark, E. Navarro-Moratalla *et al.*, "Layer-dependent ferromagnetism in a van der Waals crystal down to the monolayer limit," *Nature*, vol. 546, pp. 270–273, 2017. [Online]. Available: https://doi.org/10.1038/nature22391

[3] K. Novoselov, A. Geim, S. Morozov *et al.*, "Electric field effect in atomically thin carbon films," *Science*, vol. 306, pp. 666–669, 2004. [Online]. Available: https://doi.org/10.1126/science.110289

[4] M. Gibertini, M. Koperski, A. Morpurgo *et al.*, "Magnetic 2D materials and heterostructures," *Nat. Nanotechnol.*, vol. 14, pp. 408–419, 2019. [Online]. Available: https://doi.org/10.1038/s41565-019-0438-6

[5] X. Jiang, Q. Liu, J. Xing *et al.*, "Recent progress on 2D magnets: Fundamental mechanism, structural design and modification," *Appl. Phys. Rev.*, vol. 8, no. 3, p. 031305, 2021. [Online]. Available: https://doi.org/10.1063/5.0039979

[6] Q. Wang, A. Bedoya-Pinto, M. Blei *et al.*, "The magnetic genome of two-dimensional van der Waals materials," *ACS Nano*, vol. 16, no. 5, pp. 6960–7079, 2022. [Online]. Available: https://doi.org/10.1021/acsnano.1c09150

[7] W. He, L. Kong, W. Zhao *et al.*, "Atomically thin 2D van der Waals magnetic materials: fabrications, structure, magnetic properties and applications," *Coatings*, vol. 12, no. 2, p. 122, 2022. [Online]. Available: https://www.mdpi.com/2079-6412/12/2/122

[8] T. Lan, B. Ding, and B. Liu, "Magneto-optic effect of two-dimensional materials and related applications," *Nano Select*, vol. 1, no. 3, pp. 298–310, 2020. [Online]. Available: https://onlinelibrary.wiley.com/doi/abs/10.1002/nano.202000032

[9] P. Yang, W. Feng, G.-B. Liu *et al.*, "Giant magneto-optical Schäfer-Hubert effect in the two-dimensional van der Waals antiferromagnets $M\mathrm{PS_3}$ ($M = \mathrm{Mn}$, Fe, Ni)," *Phys. Rev. B*, vol. 107, p. 214437, 2023. [Online]. Available: https://link.aps.org/doi/10.1103/PhysRevB.107.214437

[10] Z. Wang, T. Zhang, M. Ding *et al.*, "Electric-field control of magnetism in a few-layered van der Waals ferromagnetic semiconductor," *Nat. Nanotechnol.*, vol. 13, no. 7, pp. 554–559, 2018. [Online]. Available: https://www.nature.com/articles/s41565-018-0186-z

[11] Z. Fei, B. Huang, P. Malinowski *et al.*, "Two-dimensional itinerant ferromagnetism in atomically thin $\mathrm{Fe_3GeTe_2}$," *Nature Mater*, vol. 17, pp. 778–782, 2018. [Online]. Available: https://www.nature.com/articles/s41563-018-0149-7

[12] Z. Ma, W. Zhu, G. Lin *et al.*, "Micro-MOKE with optical interference in the study of 2D $\mathrm{Cr_2Ge_2Te_6}$ nanoflake based magnetic heterostructures," *AIP Advances*, vol. 9, no. 12, p. 125116, 2019. [Online]. Available: https://doi.org/10.1063/1.5126944

[13] V. Gupta, T. Cham, G. Stiehl *et al.*, "Manipulation of the van der Waals Magnet $\mathrm{Cr_2Ge_2Te_6}$ by Spin-Orbit Torques," *Nano Lett.*, vol. 20, no. 10, pp. 7482–7488, 2020. [Online]. Available: https://doi.org/10.1021/acs.nanolett.0c02965

[14] C. Jin, Z. Tao, K. Kang *et al.*, "Imaging and control of critical fluctuations in two-dimensional magnets," *Nature Mater*, vol. 19, pp. 1290–1294, 2020. [Online]. Available: https://doi.org/10.1038/s41563-020-0706-8

[15] A. Purbawati, J. Coraux, J. Vogel *et al.*, "In-Plane magnetic domains and Néel-like domain walls in thin flakes of the room temperature $\mathrm{CrTe_2}$ van der Waals ferromagnet," *ACS Appl. Mat. Interf.*, vol. 12, no. 27, pp. 30 702–30 710, 2020. [Online]. Available: https://doi.org/10.1021/acsami.0c07017

[16] F. Hendriks and M. Guimaraes, "Enhancing magneto-optic effects in two-dimensional magnets by thin-film interference," *AIP Advances*, vol. 11, no. 3, p. 035132, 03 2021. [Online]. Available: https://doi.org/10.1063/5.0040262

[17] T. Song, Q.-C. Sun, E. Anderson *et al.*, "Direct visualization of magnetic domains and moiré magnetism in twisted 2D magnets," *Science*, vol. 374, pp. 1140–1144, 2021. [Online]. Available: https://www.science.org/doi/10.1126/science.abj7478

[18] S. Yin, L. Zhao, C. Song *et al.*, "Evolution of domain structure in $\mathrm{Fe_3GeTe_2}$," *Chinese Physics B*, vol. 30, no. 2, p. 027505, 2021. [Online]. Available: http://cpb.iphy.ac.cn

[19] A. Llacsahuanga Allcca, H. Idzuchi, X. Pan *et al.*, "Modified magnetism in heterostructures of $\mathrm{Cr_2Ge_2Te_6}$ and oxides," *AIP Advances*, vol. 13, no. 1, p. 015031, 01 2023. [Online]. Available: https://doi.org/10.1063/9.0000413

[20] C. Tan, J. Lee, S.-G. Jung *et al.*, "Hard magnetic properties in nanoflake van der Waals $\mathrm{Fe_3GeTe_2}$," *Nat Commun*, vol. 9, p. 1554, 2018. [Online]. Available: https://www.nature.com/articles/s41467-018-04018-w

[21] J. Chen, L. Wang, M. Zhang *et al.*, "Evidence for magnetic skyrmions at the interface of ferromagnet/topological-insulator heterostructures," *Nano Lett.*, vol. 19, pp. 6144–6151, 2019. [Online]. Available: https://doi.org/10.1021/acs.nanolett.9b02191

[22] Y. Wu, S. Zhang, J. Zhang *et al.*, "Néel-type skyrmion in $WTe_2/Fe_3GeTe_2$ van der Waals heterostructure," *Nat Commun*, vol. 11, p. 3860, 2020. [Online]. Available: https://doi.org/10.1038/s41467-020-17566-x

[23] V. Ostwal, T. Shen, and J. Appenzeller, "Efficient spin-orbit torque switching of the semiconducting van der Waals ferromagnet $Cr_2Ge_2Te_6$," *Adv. Mater.*, vol. 32, no. 7, p. 1906021, 2020. [Online]. Available: https://onlinelibrary.wiley.com/doi/abs/10.1002/adma.201906021

[24] Y. Wu, B. Francisco, Z. Chen *et al.*, "A van der Waals interface hosting two groups of magnetic skyrmions," *Adv. Mater.*, vol. 34, no. 16, p. 2110583, 2022. [Online]. Available: https://onlinelibrary.wiley.com/doi/abs/10.1002/adma.202110583

[25] M.-G. Han, J. Garlow, Y. Liu *et al.*, "Topological magnetic-spin textures in two-dimensional van der Waals $Cr_2Ge_2Te_6$," *Nano Lett.*, vol. 19, no. 11, pp. 7859–7865, 2019. [Online]. Available: https://doi.org/10.1021/acs.nanolett.9b02849

[26] M. Yang, Q. Li, R. Chopdekar *et al.*, "Creation of skyrmions in van der Waals ferromagnet $Fe_3GeTe_2$ on $(Co/Pd)_n$ superlattice," *Science Advances*, vol. 6, no. 36, p. eabb5157, 2020. [Online]. Available: https://www.science.org/doi/abs/10.1126/sciadv.abb5157

[27] H. Wang, C. Wang, Z.-A. Li *et al.*, "Characteristics and temperature-field-thickness evolutions of magnetic domain structures in van der Waals magnet $Fe_3GeTe_2$ nanolayers," *Appl. Phys. Lett.*, vol. 116, no. 19, p. 192403, 2020. [Online]. Available: https://doi.org/10.1063/5.0009484

[28] B. Ding, Z. Li, G. Xu *et al.*, "Observation of magnetic skyrmion bubbles in a van der Waals ferromagnet $Fe_3GeTe_2$," *Nano Lett.*, vol. 20, no. 2, pp. 868–873, 2020. [Online]. Available: https://doi.org/10.1021/acs.nanolett.9b03453

[29] Y. Gao, Q. Yin, Q. Wang *et al.*, "Spontaneous (anti)meron chains in the domain walls of van der Waals ferromagnetic $Fe_{5-x}GeTe_2$," *Adv. Mater.*, vol. 32, no. 48, p. 2005228, 2020. [Online]. Available: https://onlinelibrary.wiley.com/doi/abs/10.1002/adma.202005228

[30] T.-E. Park, L. Peng, J. Liang *et al.*, "Néel-type skyrmions and their current-induced motion in van der Waals ferromagnet-based heterostructures," *Phys. Rev. B*, vol. 103, p. 104410, 2021. [Online]. Available: https://link.aps.org/doi/10.1103/PhysRevB.103.104410

[31] Y. Gao, S. Yan, Q. Yin *et al.*, "Manipulation of topological spin configuration via tailoring thickness in van der Waals ferromagnetic $Fe_{5-x}GeTe_2$," *Phys. Rev. B*, vol. 105, p. 014426, Jan 2022. [Online]. Available: https://link.aps.org/doi/10.1103/PhysRevB.105.014426

[32] A. McCray, Y. Li, E. Qian *et al.*, "Direct observation of magnetic bubble lattices and magnetoelastic effects in van der Waals $Cr_2Ge_2Te_6$," *Adv. Funct. Mat.*, vol. 33, p. 2214203, 2023. [Online]. Available: https://onlinelibrary.wiley.com/doi/abs/10.1002/adfm.202214203

[33] C. Zhang, Z. Jiang, J. Jiang *et al.*, "Above-room-temperature chiral skyrmion lattice and Dzyaloshinskii-Moriya interaction in a van der Waals ferromagnet $Fe_3 - xGaTe_2$," *Nat Commun*, vol. 15, p. 4472, 2024. [Online]. Available: https://doi.org/10.1038/s41467-024-48799-9

[34] J. Thomsen, M.-G. Han, A. Penn *et al.*, "Effect of surface oxidation and crystal thickness on the magnetic properties and magnetic domain structures of $Cr_2Ge_2Te_6$," *ACS Nano*, vol. 18, no. 21, pp. 13 458–13 467, 2024. [Online]. Available: https://doi.org/10.1021/acsnano.3c09858

[35] L. Thiel, Z. Wang, M. Tschudin *et al.*, "Probing magnetism in 2D materials at the nanoscale with single-spin microscopy," *Science*, vol. 364, no. 6444, pp. 973–976, 2019. [Online]. Available: https://www.science.org/doi/10.1126/science.aav6926

[36] D. Abdul-Wahab, E. Iacocca, R. Evans *et al.*, "Domain wall dynamics in two-dimensional van der Waals ferromagnets," *Appl. Phys. Rev.*, vol. 8, no. 4, p. 041411, 2021. [Online]. Available: https://doi.org/10.1063/5.0062541

[37] Q.-C. Sun, T. Song, E. Anderson *et al.*, "Magnetic domains and domain wall pinning in atomically thin $CrBr_3$ revealed by nanoscale imaging," *Nat Commun*, vol. 12, p. 1989, 2021. [Online]. Available: https://doi.org/10.1038/s41467-021-22239-4

[38] R. Fujita, P. Bassirian, Z. Li *et al.*, "Layer-dependent magnetic domains in atomically thin $Fe_5GeTe_2$," *ACS Nano*, vol. 16, no. 7, pp. 10 545–10 553, 2022. [Online]. Available: https://doi.org/10.1021/acsnano.2c01948

[39] M. Birch, L. Powalla, S. Wintz *et al.*, "History-dependent domain and skyrmion formation in 2D van der Waals magnet $Fe_3GeTe_2$," *Nat Commun*, vol. 13, p. 3035, 2022. [Online]. Available: https://doi.org/10.1038/s41467-022-30740-7

[40] L. Powalla, M. Birch, K. Litzius *et al.*, "Skyrmion and skyrmionium formation in the two-dimensional magnet $Cr_2Ge_2Te_6$," *Phys. Rev. B*, vol. 108, p. 214417, 2023. [Online]. Available: https://link.aps.org/doi/10.1103/PhysRevB.108.214417

[41] A. Noah, H. Alpern, S. Singh *et al.*, "Interior and edge magnetization in thin exfoliated $CrGeTe_3$ films," *Nano Letters*, vol. 22, no. 7, pp. 3165–3172, 2022. [Online]. Available: https://doi.org/10.1021/acs.nanolett.1c04665

[42] G. Vértesy, "Coercive properties of magnetic garnet films," *Crystals*, vol. 13, no. 6, p. L012026, 2023. [Online]. Available: https://www.mdpi.com/2073-4352/13/6/946

[43] C.-K. Li, X.-P. Yao, and G. Chen, "Writing and deleting skyrmions with electric fields in a multiferroic heterostructure," *Phys. Rev. Res.*, vol. 3, p. L012026, Mar 2021. [Online]. Available: https://link.aps.org/doi/10.1103/PhysRevResearch.3.L012026

[44] D. Li, S. Haldar, and S. Heinze, "Strain-driven zero-field near-10 nm skyrmions in two-dimensional van der Waals heterostructures," *Nano Letters*, vol. 22, no. 18, pp. 7706–7713, 2022. [Online]. Available: https://doi.org/10.1021/acs.nanolett.2c03287

[45] K. Huang, D.-F. Shao, and E. Tsymbal, "Ferroelectric control of magnetic skyrmions in two-dimensional van der Waals heterostructures," *Nano Letters*, vol. 22, no. 8, pp. 3349–3355, 2022. [Online]. Available: https://doi.org/10.1021/acs.nanolett.2c00564

[46] R. Schäfer and J. McCord, *Magneto-Optical Microscopy*. Cham: Springer International Publishing, 2021, pp. 171–229.

[47] I. Soldatov and R. Schäfer, "Advanced MOKE magnetometry in wide-field Kerr-microscopy," *J. Appl. Phys.*, vol. 122, no. 15, p. 153906, 2017. [Online]. Available: https://doi.org/10.1063/1.5003719

[48] M. Khela, M. Dabrowski, S. Khan *et al.*, "Laser-induced topological spin switching in a 2D van der Waals magnet," *Nat Commun*, vol. 14, p. 1378, 2023. [Online]. Available: https://doi.org/10.1038/s41467-023-37082-y

[49] V. Carteaux, D. Brunet, G. Ouvrard *et al.*, "Crystallographic, magnetic and electronic structures of a new layered ferromagnetic compound $Cr_2Ge_2Te_6$," *J. Phys.: Condens. Matter*, vol. 7, no. 1, p. 69, 1995. [Online]. Available: http://dx.doi.org/10.1088/0953-8984/7/1/008

[50] S. Selter, G. Bastien, A. Wolter *et al.*, "Magnetic anisotropy and low-field magnetic phase diagram of the quasi-two-dimensional ferromagnet $Cr_2Ge_2Te_6$," *Phys. Rev. B*, vol. 101, p. 014440, 2020. [Online]. Available: https://link.aps.org/doi/10.1103/PhysRevB.101.014440

[51] X. Zhang, Y. Zhao, Q. Song *et al.*, "Magnetic anisotropy of the single-crystalline ferromagnetic insulator $Cr_2Ge_2Te_6$," *Japanese Journal of Applied Physics*, vol. 55, no. 3, p. 033001, 2016. [Online]. Available: https://dx.doi.org/10.7567/JJAP.55.033001

[52] J. Zeisner, A. Alfonsov, S. Selter *et al.*, "Magnetic anisotropy and spin-polarized two-dimensional electron gas in the van der Waals ferromagnet $Cr_2Ge_2Te_6$," *Phys. Rev. B*, vol. 99, p. 165109, 2019. [Online]. Available: https://link.aps.org/doi/10.1103/PhysRevB.99.165109

[53] I. V. Soldatov and R. Schäfer, "Selective sensitivity in Kerr microscopy," *Rev. Scient. Instr.*, vol. 88, no. 7, p. 073701, 2017. [Online]. Available: https://doi.org/10.1063/1.4991820

[54] F. Schmidt and A. Hubert, "Domain observations on CoCr-layers with a digitally enhanced Kerr-microscope," *J. Magn. Magn. Mater.*, vol. 61, no. 3, pp. 307 – 320, 1986. [Online]. Available: http://www.sciencedirect.com/science/article/pii/0304885386900442

[55] W. Kuch, R. Schäfer, P. Fischer, and F. Hillebrecht, *Magnetic Microscopy of Layered Structures*. Berlin Heidelberg: Springer-Verlag, 2015. [Online]. Available: https://doi.org/10.1007/978-3-662-44532-7

[56] R. Schäfer, *Magnetic Domains*. Cham: Springer International Publishing, 2020, pp. 1–44.

[57] A. Hubert and R. Schäfer, *Magnetic Domains: The Analysis of Magnetic Microstructures*. Berlin Heidelberg: Springer-Verlag, 1998. [Online]. Available: https://www.springer.com/gp/book/9783540641087

[58] C. Kittel, "Theory of the Structure of Ferromagnetic Domains in Films and Small Particles," *Physical Review*, vol. 70, no. 11, pp. 965–971, 1946. [Online]. Available: https://doi.org/10.1103/PhysRev.70.965

[59] Z. Máleck and V. Kamberský, "On the theory of the domain structure of thin films of magnetically uni-axial materials," *Czech. Journ. Phys.*, vol. 8, pp. 416–421, 1958. [Online]. Available: https://link.springer.com/article/10.1007/BF01612066

[60] C. Kooy and U. Enz, "Experimental and theoretical study of the domain configuration in thin layers of $BaFe_{12}O_{19}$," *Philips Res. Repts*, vol. 15, pp. 7–29, 1960.

[61] Y. Fang, S. Wu, Z. Zhu, and others., "Large magneto-optical effects and magnetic anisotropy energy in two-dimensional $Cr_2Ge_2Te_6$," *Phys. Rev. B*, vol. 98, p. 125416, 2018. [Online]. Available: https://link.aps.org/doi/10.1103/PhysRevB.98.125416

[62] C. Song, X. Liu, X. Wu *et al.*, "Surface-vacancy-induced metallicity and layer-dependent magnetic anisotropy energy in $Cr_2Ge_2Te_6$," *J. Appl. Phys.*, vol. 126, no. 10, p. 105111, 2019. [Online]. Available: https://doi.org/10.1063/1.5109875

[63] Y. Yafet and E. M. Gyorgy, "Ferromagnetic strip domains in an atomic monolayer," *Phys. Rev. B*, vol. 38, pp. 9145–9151, Nov 1988. [Online]. Available: https://link.aps.org/doi/10.1103/PhysRevB.38.9145

[64] R. Allenspach, "Ultrathin films: magnetism on the microscopic scale," *J. Magn. Magn. Mat.*, vol. 129, pp. 160–185, 1994. [Online]. Available: https://www.sciencedirect.com/science/article/pii/0304885394901082

[65] G. Träger, L. Wenzel, and A. Hubert, "Computer experiments on the information depth and the figure of merit in magnetooptics," *phys. stat. sol. (a)*, vol. 131, no. 1, pp. 201–227, 1992. [Online]. Available: http://dx.doi.org/10.1002/pssa.2211310131

[66] R. Schäfer, P. Oppeneer, A. Ognev *et al.*, "Analyzer-free, intensity-based, wide-field magneto-optical microscopy," *Applied Physics Reviews*, vol. 8, no. 3, p. 031402, 2021. [Online]. Available: https://doi.org/10.1063/5.0051599

[67] A. Hubert and G. Träger, "Magneto-optical sensitivity functions of thin-film systems," *J. Magn. Magn. Mater.*, vol. 124, no. 1-2, pp. 185 – 202, 1993. [Online]. Available: http://www.sciencedirect.com/science/article/pii/030488539390087I

[68] H. Idzuchi, A. Llacsahuanga Allcca, A. Haglund *et al.*, "On the optical properties of $Cr_2Ge_2Te_6$ and its heterostructure," *Cond. Matter*, vol. 8, no. 3, p. 59, 2023. [Online]. Available: https://www.mdpi.com/2410-3896/8/3/59

[69] J. Pearson, P. T. Squire, and D. Atkinson, "Which anhysteretic magnetization curve?" *IEEE Trans. Magn.*, vol. 33, no. 5, pp. 3970–3972, 1997. [Online]. Available: https://ieeexplore.ieee.org/document/619632

[70] G. Gerritsma, M. W. Stam, J. Lodder *et al.*, "Initial slope of the hysteresis curve," *J. Phys. Colloqu.*, vol. 49, no. C8, pp. 1997–1998, 1988. [Online]. Available: https://doi.org/10.1051/jphyscol:19888906

[71] T. Guo, Z. Ma, X. Luo *et al.*, "Multiple domain structure and symmetry types in narrow temperature and magnetic field ranges in layered $Cr_2Ge_2Te_6$crystal measured by magnetic force microscope," *Materials Characterization*, vol. 173, p. 110913, 2021. [Online]. Available: https://www.sciencedirect.com/science/article/pii/S1044580321000437

[72] N. Leon-Brito, E. Bauer, F. Ronning *et al.*, "Magnetic microstructure and magnetic properties of uniaxial itinerant ferromagnet $Fe_3GeTe_2$," *J. of Appl. Phys.*, vol. 120, no. 8, p. 083903, 2016. [Online]. Available: https://doi.org/10.1063/1.4961592

[73] J. Yi, H. Zhuang, Q. Zou *et al.*, "Competing antiferromagnetism in a quasi-2D itinerant ferromagnet: $Fe_3GeTe_2$," *2D Materials*, vol. 4, no. 1, p. 011005, 2016. [Online]. Available: https://dx.doi.org/10.1088/2053-1583/4/1/011005

[74] J. Goodenough, "Interpretation of domain patterns recently found in BiMn and SiFe alloys'," *Phys. Rev.*, vol. 102, no. 2, pp. 356–365, 1956. [Online]. Available: https://doi.org/10.1103/PhysRev.102.356

[75] R. Cowburn, D. Koltsov, A. Adeyeye *et al.*, "Single-Domain Circular Nanomagnets," *Phys. Rev. Lett.*, vol. 83, pp. 1042–1045, 1999. [Online]. Available: https://link.aps.org/doi/10.1103/PhysRevLett.83.1042

[76] I. Soldatov, P. Andrei, and R. Schäfer, "Inverted Hysteresis, Magnetic Domains, and Hysterons," *IEEE Magn. Lett.*, vol. 11, pp. 1–5, 2020. [Online]. Available: 10.1109/LMAG.2020.3035136

[77] R. Schäfer and A. Desimone, "Hysteresis in soft ferromagnetic films: experimental observations and micromagnetic analysis," *IEEE Trans. Magne.*, vol. 38, no. 5, pp. 2391–2393, 2002. [Online]. Available: 10.1109/TMAG.2002.803592

[78] J. E. Davies, O. Hellwig, Fullerton *et al.*, "Magnetization reversal of $Co/Pt$ multilayers: Microscopic origin of high-field magnetic irreversibility," *Phys. Rev. B*, vol. 70, p. 224434, 2004. [Online]. Available: https://link.aps.org/doi/10.1103/PhysRevB.70.224434

[79] E. A. Jagla, "Hysteresis loops of magnetic thin films with perpendicular anisotropy," *Phys. Rev. B*, vol. 72, p. 094406, 2005. [Online]. Available: https://link.aps.org/doi/10.1103/PhysRevB.72.094406

[80] J. M. Deutsch and T. Mai, "Mechanism for nonequilibrium symmetry breaking and pattern formation in magnetic films," *Phys. Rev. E*, vol. 72, p. 016115, 2005. [Online]. Available: https://link.aps.org/doi/10.1103/PhysRevE.72.016115

[81] M. S. Pierce, C. R. Buechler, Sorensen *et al.*, "Disorder-induced microscopic magnetic memory," *Phys. Rev. Lett.*, vol. 94, p. 017202, 2005. [Online]. Available: https://link.aps.org/doi/10.1103/PhysRevLett.94.017202

[82] L. Ma, D. A. Gilbert, V. Neu *et al.*, "Magnetization reversal in perpendicularly magnetized $L1_0$ FePd/FePt heterostructures," *J. Appl. Phys.*, vol. 116, p. 033922, 2014. [Online]. Available: https://doi.org/10.1063/1.4890936

[83] O. Maximova, S. Lyaschenko, I. Tarasov *et al.*, "The magneto-optical Voigt parameter from magneto-optical ellipsometry data for multilayer samples with single ferromagnetic layer," *Physics of the Solid State*, vol. 63, pp. 1485–1495, 2021. [Online]. Available: https://ui.adsabs.harvard.edu/abs/2021PhSS...63.1485M

[84] G. Träger, L. Wenzel, A. Hubert *et al.*, "Magnetooptical effects in non-uniform magnetized media," *IEEE Trans. Magn.*, vol. 29, pp. 3408–3410, 1993. [Online]. Available: 10.1109/20.280830

[85] L. Wenzel, V. Kamberský, and A. Hubert, "A systematic first-order theory of magnetooptic diffraction in magnetic multilayers," *phys. stat. sol. (a)*, vol. 151, no. 2, pp. 449–466, 1995. [Online]. Available: http://dx.doi.org/10.1002/pssa.2211510223

[86] L. Wenzel, A. Hubert, and V. Kamberský, "Transparent simulation of magneto-optic diffraction from arbitrary magnetic multilayers," *J. Magn. Magn. Mater.*, vol. 175, pp. 205 – 211, 1997. [Online]. Available: http://www.sciencedirect.com/science/article/pii/S0304885397001595

[87] V. Kamberský, L. Wenzel, and A. Hubert, "Magneto-optical interference and diffraction in isotropic and uniaxial multilayers," *J. Magn. Magn. Mater.*, vol. 189, no. 2, pp. 149 – 164, 1998. [Online]. Available: http://www.sciencedirect.com/science/article/pii/S0304885398002145